Research Square

Preprints are preliminary reports that have not undergone peer review.
They should not be considered conclusive, used to inform clinical practice,
or referenced by the media as validated information.

Vertical Atmospheric Moisture Change Across Global Hydroclimatic Regimes During the Past 50 Years

Shanshan Xu
East China Normal University
Jie Zhang
Tianjin University
Hongming He
hmhe@geo.ecnu.edu.cn

East China Normal University

Article

Keywords:

Posted Date: November 13th, 2026

DOI: https://doi.org/10.21203/rs.3.rs-11548762/v1

License: This work is licensed under a Creative Commons Attribution 4.0 International License.
Read Full License

Additional Declarations: No competing interests reported.

Vertical Atmospheric Moisture Change Across Global Hydroclimatic Regimes During the Past 50 Years

Shanshan Xu, [a] Jie Zhang, [*, b] Hongming He[*, a]

[a] *School of Geographic Sciences, East China Normal University, Shanghai, China.*

[b] *College of Intelligence and Computing, Tianjin University, Tianjin, China.*

Corresponding author: Hongming He (Ph.D., Professor)

E-mail: hmhe@geo.ecnu.edu.cn

Abstract

The vertical structure of atmospheric moisture is important for understanding land–atmosphere interactions, energy exchange, and the hydrological cycle. However, how thermodynamic moistening potential is expressed in observed specific-humidity changes across the troposphere remains insufficiently understood. Here, we analyse monthly mean temperature and specific humidity from ERA5 for 1979–2025 across 37 pressure levels and five hydroclimatic regimes. We quantify the thermodynamic component using Clausius–Clapeyron (C–C) scaling and diagnose the remaining non-thermodynamic residual, with MERRA-2 and ERA5-Land used to assess consistency. Terrestrial atmospheric moistening exhibits pronounced vertical variations. The thermodynamic component remains positive across the analysed levels but decreases substantially with height, from approximately 0.22–0.34 g kg^{-1} decade^{-1} at 1000 hPa to 0.002–0.06 g kg^{-1} decade^{-1} at 500 hPa and near zero at 250 hPa. In the lower troposphere, negative residuals (approximately −0.30 to −0.17 g kg^{-1} decade^{-1}) substantially offset the thermodynamic component. The relative magnitude of the thermodynamic component increases toward 500 hPa, as indicated by CR values rising from 0.05–0.46 at 1000 hPa to 0.69–1.05 at 500 hPa, before becoming less distinct near 250 hPa (−0.12 to 0.34). Hydroclimatic differences reflect variations in the extent to which the residual offsets thermodynamic moistening potential. These results show that terrestrial atmospheric moisture change is not a vertically uniform response to warming. Instead, the realized specific-humidity response depends on both the thermodynamic moistening potential and its height- and regime-dependent offset by the residual. This framework provides vertically resolved constraints for evaluating atmospheric humidity changes in climate models and motivates further investigation of the physical processes underlying the residual.

Introduction

Atmospheric water vapour is a fundamental component of the climate system and a key link between the global energy and hydrological cycles. Through its strong radiative effects and its role in latent heat transport and release, water vapour regulates atmospheric energy balance while providing the moisture source for precipitation and influencing convection, clouds and large-scale atmospheric circulation (Soden et al. 2005; Held and Soden 2006; Allan et al. 2022). Its vertical distribution is particularly important because water vapour is strongly stratified through the troposphere, and changes at different levels can modify radiative cooling, atmospheric stability, convective development and the transport and redistribution of moisture. The vertical thermal structure of the atmosphere further couples moisture changes to convection and large-scale

circulation, linking thermodynamic changes in atmospheric moisture with the redistribution of water within the climate system (Bony et al. 2006; Sherwood et al. 2010; O'Gorman and Muller 2010). Recent observational and reanalysis-based studies have documented widespread changes in atmospheric water vapour during recent decades, while also revealing substantial differences among altitude levels and observing systems (Santer et al. 2007; Willett et al. 2007; Dessler and Davis 2010; Schröder et al. 2019; Allan et al. 2022). Changes in the vertical structure of atmospheric moisture therefore provide an important perspective for understanding how warming modifies the physical functioning of the global water cycle, but the mechanisms governing its height-dependent evolution remain incompletely constrained.

Changes in atmospheric moisture have consequences that extend beyond the atmospheric water cycle to terrestrial ecosystems and human water use. Through its roles in precipitation, evapotranspiration and atmospheric evaporative demand, atmospheric moisture influences the availability and redistribution of water over land. Changes in atmospheric evaporative demand, particularly rising Vapour Pressure Deficit (VPD), can constrain stomatal conductance and photosynthesis, intensify plant water stress and alter ecosystem carbon and water exchanges, with consequences for forests, grasslands and managed ecosystems (Novick et al. 2024). At broader spatial scales, changes in precipitation, evapotranspiration and terrestrial water storage modify the spatial and temporal distribution of water availability and contribute to changes in drought and wet conditions (Zaitchik et al. 2023; Rodell and Li 2023). These hydroclimatic changes have direct implications for ecosystem functioning, agricultural production and water-resource management. Yet assessments of these impacts have generally focused on surface hydroclimatic variables or integrated water availability, providing limited constraints on how vertically resolved atmospheric moisture changes contribute to terrestrial hydroclimatic variability.

The physical interpretation of atmospheric moistening has traditionally been based on the Clausius–Clapeyron (C–C) relation, which provides a thermodynamic constraint on the temperature dependence of saturation water vapour. Under approximately fixed relative humidity, saturation specific humidity increases by about 7% K^{-1} at typical tropospheric temperatures, establishing a widely used reference for the thermodynamic moisture response to warming (Held and Soden 2006; O'Gorman and Muller 2010; Allan et al. 2022; Douville et al. 2022). Observed humidity changes, do not necessarily follow this scaling because temperature-driven moisture increases interact with atmospheric circulation, moisture transport, vertical motion, relative-humidity changes, boundary-layer mixing and land-surface coupling (Sherwood et al. 2010; Byrne and O'Gorman 2015, 2018; Wills et al. 2016). Thermodynamic–non-thermodynamic decomposition frameworks have consequently been developed to distinguish temperature-related effects from other processes in studies of precipitation, evapotranspiration and hydrological-cycle changes (Seager et al. 2010; Pfahl et al. 2017). Similar approaches have provided evidence that thermodynamic and dynamical processes can exert different influences across regions and atmospheric states. Recent observational studies have also identified departures from simple thermodynamic expectations in atmospheric moisture, particularly over dry regions, while global multi-product assessments have highlighted uncertainties in the magnitude and vertical expression of observed water-vapour changes (Simpson et al. 2024; Allan and Douville 2024; Allan et al. 2022). Nevertheless, most existing attribution studies have focused on precipitation, moisture transport or column-integrated water vapour rather than the continuous vertical profile of specific humidity. Moreover, when applied to specific

humidity, the residual after removing the temperature-driven component cannot be uniquely interpreted as a circulation contribution because it integrates the effects of several processes that are not explicitly represented by the thermodynamic term. The reliability of the resulting attribution therefore depends on resolving the vertical structure of specific-humidity changes and evaluating the consistency of the inferred patterns across independent data products.

These advances establish a physical basis for interpreting atmospheric moistening, but they also point to a common limitation in current understanding. Existing studies have documented broad increases in atmospheric water vapour and clarified the thermodynamic constraint imposed by warming, while evidence from observations, reanalyses and ecosystem studies increasingly indicates that the magnitude and vertical expression of moisture change vary across atmospheric levels and hydroclimatic environments (Allan et al. 2022; Zaitchik et al. 2023; Novick et al. 2024). A vertically resolved framework is therefore needed to connect the thermodynamic moisture potential associated with warming with the specific-humidity response that is actually realized across the troposphere. Here, we address this need by analysing monthly temperature and specific humidity from ERA5 at 37 pressure levels over 1979–2025 and by comparing five hydroclimatic regimes together with Antarctica. We first characterize the vertical structure and long-term evolution of terrestrial specific humidity across the analysed troposphere. We then quantify the local thermodynamic moistening potential associated with temperature change using a C–C-based framework and evaluate the departure of the realized specific-humidity response from this thermodynamic component. We finally examine how the resulting non-thermodynamic residual varies with altitude and hydroclimatic regime, while using MERRA-2 and ERA5-Land for cross-product consistency assessment. This framework distinguishes the thermodynamic potential for moistening from its realized specific-humidity response and provides a vertically resolved basis for assessing how warming-related moisture changes vary across the terrestrial climate system.

Results

Vertical structure and long-term changes in terrestrial atmospheric moisture

Terrestrial specific humidity exhibits pronounced vertical stratification throughout the study period, decreasing with altitude and showing the highest values over humid regions and the lowest over hyperarid regions and Antarctica. Despite these differences in background moisture, a common temporal pattern emerges across hydroclimatic regimes, with positive specific-humidity anomalies becoming more pronounced after the late twentieth century, particularly in the 1000–500 hPa layer (Fig. 1).

However, the increase is not vertically uniform. The largest and most persistent positive anomalies occur in the lower and middle troposphere, whereas changes near 250 hPa remain comparatively weak. This height dependence is evident across the major hydroclimatic regimes, although the magnitude and persistence of the response vary among regions (Fig. 1b–h). Humid and dry-subhumid regions exhibit more pronounced lower- to mid-tropospheric moistening, whereas arid and semiarid regions show weaker and more variable responses.

The vertical specific-humidity gradients provide a complementary perspective on these height-

dependent changes (Fig. 2). In the 1000–850 hPa layer, the gradient strengthens across most hydroclimatic regimes, with the largest increase in the hyperarid regime (+0.03 g kg^{-1} $decade^{-1}$), followed by the semiarid (+0.01), dry-subhumid (+0.008) and arid regimes (+0.007) (Fig. 2a). Spatially, positive trends are concentrated over humid tropical and monsoon regions, while weaker or negative trends occur across several subtropical drylands and continental interiors (Fig. 2d). This pattern indicates that changes in lower-tropospheric humidity contrast vary substantially with hydroclimatic regime.

The particularly evident hydroclimatic contrast occurs in the 850–500 hPa layer. The gradient weakens markedly in the humid regime (approximately −0.075 g kg^{-1} $decade^{-1}$), whereas it changes little or increases in the drier regimes, including a positive trend in the hyperarid regime (Fig. 2a). The corresponding spatial distribution shows pronounced regional differences across tropical, subtropical and continental interiors (Fig. 2c), indicating that the middle troposphere exhibits greater hydroclimatic heterogeneity in the evolution of vertical humidity contrast than the lower layer.

In the 500–250 hPa layer, the gradient increases in several regimes, with relatively large positive trends in the hyperarid (+0.04 g kg^{-1} $decade^{-1}$) and humid (+0.03g kg^{-1} $decade^{-1}$) regimes (Fig. 2a). Given the low absolute specific humidity at these levels, these gradient changes represent changes in the vertical humidity contrast rather than moisture increases comparable in magnitude to those in the lower troposphere. Taken together, the three layers reveal a height-dependent pattern characterized by widespread lower-tropospheric gradient strengthening, pronounced hydroclimatic contrasts in the middle troposphere, and positive gradient trends in several regimes aloft. These results indicate that the long-term change in terrestrial atmospheric moisture is not vertically uniform and provide a basis for separating the temperature-driven thermodynamic component from the residual component in the subsequent analysis.

Thus, the observed response is not a simple amplification of the climatological humidity profile. Instead, warming is associated with height-dependent changes in the vertical specific-humidity response, characterized by stronger lower-level gradients, clearer hydroclimatic differences in the middle troposphere, and changes in the upper-level humidity gradient. This vertical heterogeneity motivates separating the temperature-driven thermodynamic component from the processes that modulate its realization.

Hydroclimatic-regime departures of realized specific-humidity responses from C–C scaling

To assess whether observed atmospheric moistening follows the Clausius–Clapeyron (C–C) thermodynamic constraint, we expressed specific-humidity trends as moistening responses relative to the local C–C scaling and conducted independent evaluations using MERRA-2 reanalysis data and the ERA5-Land near-surface product (Fig. 3). Santer et al. (2007) established an anthropogenic signal of global moistening, but whether this signal follows a single thermodynamic scaling law throughout the troposphere remains to be investigated (Santer et al., 2007). Our results show that the moistening response generally increases with warming but remains below the theoretical C–C

expectation, with the degree of deviation exhibiting clear vertical dependence and differences among hydroclimatic regimes.

ERA5 and MERRA-2 reproduce similar vertical patterns of deviation (Fig. 3a). In the lower atmosphere (within the planetary boundary layer), the realized moistening response approaches but generally remains below the local C–C scaling. The deviation becomes larger in the free troposphere, with more pronounced regional differences in the middle and upper troposphere. The moistening response is weakest in the upper troposphere, around 250 hPa, where its departure from the local C–C scaling is also greatest. Soden et al. (2005) highlighted the substantial radiative effects associated with upper-tropospheric water-vapour increases (Soden et al., 2005). The results show that the absolute magnitude of long-term moistening at this level is much smaller than that in the lower troposphere. Therefore, assessments of upper-tropospheric water-vapour feedback should not rely solely on absolute increases; relative rates of change may provide a more sensitive indicator.

The vertical dependence is important. The largest deviation occur in the lower troposphere, where the realized moistening rate remains substantially below the local thermodynamic expectation. At 1000 hPa, the deviation reaches approximately 3.93 % K^{-1} in the Hyperarid regime, compared with a C–C expectation of 7 % K^{-1}. Around the middle troposphere, the departure becomes smaller, and the normalized response at 500 hPa is closer to the local thermodynamic expectation, although substantial hydroclimatic differences remain (Fig. 3a). Near 250 hPa, the relative response becomes more variable because the absolute magnitude of specific-humidity changes is small.

The multi-product comparison further supports the consistency of the lower-tropospheric signal. MERRA-2 reproduces the principal vertical structure identified by ERA5, while ERA5-Land shows strong spatial consistency with ERA5 in specific-humidity trends at the 1000-hPa level, with grid-cell correlations exceeding 0.95 and trend agreement exceeding 90% (Fig. 3b–d). The differences are concentrated mainly over complex terrain and regions with strong land-surface gradients, whereas the spatial patterns are broadly consistent across most terrestrial areas. Because ERA5-Land uses ERA5 atmospheric forcing, this comparison is interpreted as a multi-product consistency assessment rather than validation based on three fully independent datasets. Together, these results suggest a distinction between thermodynamic moistening and the realized specific-humidity response.

Height-dependent thermodynamic and residual components of atmospheric moisture change

The thermodynamic component and non-thermodynamic residual exhibit contrasting spatial patterns across terrestrial regions, with corresponding differences in the realized specific-humidity trends (Fig. 4a–g). At 1000 hPa, the thermodynamic component is positive across the major hydroclimatic regimes, with regime-mean values of approximately +0.22 to +0.34 g kg^{-1} $decade^{-1}$, indicating widespread thermodynamic moistening potential. The residual, by contrast, is negative across many continental interiors, particularly in dry regions. This contrast is also evident in specific geographic regions: the thermodynamic component is partly offset by a negative residual over the Arabian Peninsula and the Sahara, whereas the spatial patterns of the realized specific-humidity

trends vary across other regions, including the Congo Basin, South Asian monsoon region, Amazon Basin, and interior Australia. These patterns indicate that the realized humidity response does not necessarily follow the spatial distribution of the thermodynamic component alone.

The vertical profiles further show that the relative magnitudes of the two components vary with height (Fig. 4h). At 1000 hPa, the negative non-thermodynamic residual substantially offsets the positive thermodynamic component, reducing the realized increase in specific humidity relative to the thermodynamic component alone. In the Arabian Peninsula regime, a thermodynamic component of approximately +0.37 g kg^{-1} $decade^{-1}$ is largely offset by a residual of −0.21 g kg^{-1} $decade^{-1}$. In the Sahara Desert regime, the thermodynamic component is larger (+0.33 g kg^{-1} $decade^{-1}$), while the residual remains strongly negative (−0.26 g kg^{-1} $decade^{-1}$), leaving a positive but substantially smaller realized increase of approximately +0.08 g kg^{-1} $decade^{-1}$. At 850 hPa, this compensating pattern persists but the residual weakens. By 500 hPa, the global land-mean residual has declined to approximately −0.013 g kg^{-1} $decade^{-1}$, allowing the realized response to more closely follow the positive thermodynamic component. Near 250 hPa, both components are small and the net specific-humidity trend approaches zero. This compensating relationship weakens with height as the residual decreases, allowing the realized specific-humidity response to more closely reflect the thermodynamic component around 500 hPa.

The residual is defined as the difference between the observed specific-humidity trend and the thermodynamic component. It therefore represents the aggregate of effects not captured by the thermodynamic component, rather than the independently estimated contribution of a single dynamical process.

Hydroclimatic dependence of the vertical thermodynamic–residual balance

This figure aims to reveal a consistent and systematic height dependence in the thermodynamic–non-thermodynamic balance across hydroclimatic regimes. We quantify the thermodynamic component and non-thermodynamic residual at 1000, 850, 500, and 250 hPa using two complementary diagnostics: the thermodynamic–residual mean difference index (TMI) and the component magnitude ratio (CR) (Fig. 5). The thermodynamic component remains positive across all regimes, whereas the residual magnitude varies strongly with both regime and height. This indicates that regional differences in realized moistening are controlled mainly by residual modulation rather than by changes in the thermodynamic response itself.

The hydroclimatic regimes differ in the extent to which the thermodynamic component is offset by the non-thermodynamic residual (Fig. 5). At 1000 hPa, the hyperarid regime has a thermodynamic component of approximately +0.34 g kg^{-1} $decade^{-1}$ and a residual of −0.24 g kg^{-1} $decade^{-1}$, yielding a net specific-humidity increase of approximately +0.10–0.11 g kg^{-1} $decade^{-1}$. In the arid and semiarid regimes, thermodynamic components of approximately +0.31 and +0.27

g kg^{-1} decade^{-1} are partly offset by residuals of −0.27 and −0.22 g kg^{-1} decade^{-1}, respectively. In the humid regime, the thermodynamic component is smaller (+0.23 g kg^{-1} decade^{-1}) and is also largely offset by a negative residual (−0.21 g kg^{-1} decade^{-1}). Thus, despite differences in the magnitude of the thermodynamic component, the realized near-surface humidity trends are moderated to varying degrees by the residual.

These comparisons show that the thermodynamic component alone does not fully account for differences in realized moistening among hydroclimatic regimes. In particular, the hyperarid regime retains a positive net trend despite a substantial negative residual, whereas the smaller thermodynamic component in the humid regime is also accompanied by a negative residual of comparable magnitude. The resulting trends therefore depend on both the magnitude of the thermodynamic component and the extent to which it is offset by the residual.

The relative-magnitude diagnostics provide a complementary perspective on the balance between the thermodynamic component and the non-thermodynamic residual across pressure levels (Fig. 6a). The contribution ratio (CR), defined as the logarithm of the ratio of their absolute magnitudes, increases from approximately 0.05–0.46 at 1000 hPa to 0.69–1.05 around 500 hPa, before decreasing to −0.12–0.34 at 250 hPa. The absolute-magnitude weight of the thermodynamic component (W_{Thermo}) shows a broadly consistent vertical pattern. Together, these indices indicate that the thermodynamic component becomes relatively larger than the residual toward the middle troposphere, whereas their relative magnitudes become more comparable or less clearly differentiated near the upper level.

These indices complement the component values shown in Fig. 5 by distinguishing relative magnitude from the net response. A relatively large W_{Thermo} does not necessarily imply a large positive specific-humidity trend, because the realized response also depends on the absolute magnitudes and signs of both components. Conversely, a small net trend may result from the offsetting of two components that are individually larger than their sum. CR and W_{Thermo} therefore characterize the relative balance between the two terms, rather than directly quantifying the magnitude or sign of the realized humidity trend.

The synthesis in Fig. 6b summarizes three broad vertical features: substantial thermodynamic–residual compensation in the lower troposphere, a relatively larger thermodynamic component around the middle troposphere, and small component magnitudes with a weak net response near 250 hPa. These features provide a compact interpretation of the relationships identified in Figs. 4 and 5. They should be understood as a summary of the diagnosed component balance, rather than as evidence for distinct physical regimes or a uniquely identified dynamical mechanism. Because the residual is calculated as the difference between the observed trend and the thermodynamic component, its physical interpretation remains aggregate.

Discussion

Height-dependent expression of thermodynamic moistening in terrestrial

atmospheric moisture

Our results indicate a distinction between thermodynamic moisture potential and realized terrestrial atmospheric moistening. Warming establishes a broadly positive thermodynamic component across the analysed troposphere, but the observed specific-humidity response does not increase proportionally across levels. Instead, the degree to which the thermodynamic potential is realized changes systematically with height (Fig. 3a; Fig. 4e–f).

This interpretation is consistent with observational studies documenting vertical differences in tropospheric humidity changes and departures from simple Clausius–Clapeyron (C–C) scaling (Dessler and Davis 2010; Chung et al. 2014; Allan et al. 2022). Recent work by Cao et al. (2026) further demonstrates that temperature-related moistening and moisture-supply-related changes can partially offset one another, producing regionally contrasting atmospheric water-vapour anomalies during Northern Hemisphere summer heatwaves(Cao et al. 2026). Their analysis focuses on interannual variability in heatwave-related column water vapour and its radiative effects, whereas the present study examines long-term specific-humidity trends at fixed pressure levels over land. The two studies therefore address different aspects of atmospheric moisture change, but together underscore the value of distinguishing temperature-related moisture responses from the humidity changes that are actually realized.

The hydroclimatic contrasts identified here also suggest that a single C–C scaling relationship is insufficient to describe the full spatial and vertical structure of terrestrial specific-humidity trends. At lower levels, regions with different moisture regimes can exhibit substantial differences between the thermodynamic component and the realized response, whereas the correspondence becomes closer around the middle troposphere (Figs. 3a and 5). This result is broadly consistent with studies emphasizing that land humidity is affected not only by local thermodynamic conditions but also by atmospheric circulation, moisture transport and land-surface processes (Sherwood et al. 2010; Dessler and Davis 2010; Byrne and O'Gorman 2015, 2018). By examining fixed pressure levels across five hydroclimatic regimes, this study extends the assessment of moisture responses beyond near-surface or column-integrated measures. The results indicate that departures from the temperature-related reference vary systematically with height, although the present decomposition does not independently identify the physical processes responsible for those departures.

Hydroclimatic contrasts in thermodynamic–residual balance

The hydroclimatic contrasts indicate that differences in realized moistening are associated particularly with the magnitude of the residual in the lower troposphere (Figs. 4–6). Dry regimes provide a notable example: despite relatively large thermodynamic components near the surface, negative residuals reduce the realized humidity response (Fig. 5). This pattern is broadly consistent with recent observational evidence that moisture increases over dry regions may be smaller than those simulated by climate models (Simpson et al. 2024), although the present decomposition addresses a different question by quantifying the departure from the local temperature-driven component.

Broader changes in hydroclimatic conditions also occur at scales that are not captured by the present decomposition. Chemke and Grise (2025) identified an autumnal poleward shift of the Northern Hemisphere tropical hydrological-cycle edge that emerged beyond the range of internal variability, with evidence supporting an anthropogenic influence. It provides broader context for regional hydroclimatic change, rather than direct evidence for the vertical patterns diagnosed here. The spatial distribution of the residual is heterogeneous across land. Negative residuals are widespread over many continental interiors, whereas weaker or positive residuals occur in some regions with stronger moisture transport or monsoonal influence (Fig. 4f–g). Such spatial variability is consistent with the potential influence of moisture transport, circulation and land-surface processes on regional humidity. However, the residual defined here as Total minus Thermo does not distinguish among these processes. Previous studies provide evidence that these processes can influence terrestrial humidity and relative-humidity changes (Vicente-Serrano et al. 2018; Douville et al. 2020; Kim and Johnson 2025; Ding et al. 2026), but they cannot be uniquely separated using the present decomposition. Process-based studies also demonstrate that moisture-budget responses can vary considerably across seasons and external forcing. For example, Choi et al. (2023) found distinct seasonal contributions of poleward moisture transport and surface evaporation to historical Arctic hydroclimatic changes under different forcing experiments. Independent studies have shown that changes in atmospheric vertical motion can substantially influence hydrological responses under warming (Jun and Rind 2024). These findings provide context for the potential range of processes affecting atmospheric moisture, but they do not identify the cause of the residual in the present study. Because the residual is calculated as the difference between the observed specific-humidity trend and the temperature-related thermodynamic component, it remains a diagnostic remainder rather than an independently estimated moisture-budget term. Assigning it directly to circulation, evaporation or any other individual process would therefore exceed the evidence provided by this decomposition.

The vertical evolution of the relative component magnitude provides an additional synthesis of this contrast. The increasing thermodynamic weight toward the middle troposphere is associated mainly with the weakening residual rather than with a change in the drection of the thermodynamic component (Fig. 6a). The three response zones illustrated in Fig. 6b should therefore be viewed as a conceptual summary of the diagnosed component magnitudes, rather than as evidence for three independently identified physical regimes. In this sense, the main hydroclimatic difference identified here concerns the degree of residual modulation of the thermodynamic potential, rather than a reversal of the thermodynamic response itself.

The consistency among ERA5, MERRA-2 and ERA5-Land provides some support for the robustness of the broad pattern, particularly for the lower-tropospheric signal (Fig. 3b–d). Nevertheless, these products are not fully independent observational records, and differences in assimilation systems, observational constraints and data coverage can contribute to uncertainty in long-term humidity estimates (Allan et al. 2022). The multi-product comparison therefore strengthens confidence in the diagnosed spatial and vertical structure but does not remove uncertainty in its magnitude or physical interpretation.

Implications for interpreting terrestrial moisture change

The results indicate that near-surface and column-integrated humidity metrics may not fully represent the vertical differences between temperature-related thermodynamic responses and realized specific-humidity trends. A vertically resolved decomposition can instead distinguish the positive temperature-driven component from the residual modulation, providing an additional diagnostic for evaluating whether models reproduce the observed vertical structure of humidity change (Figs. 4–6). Evaluating the vertical structure is therefore necessary for distinguishing a genuine thermodynamic response from a response shaped by compensating non-thermodynamic processes.

The vertical structure of atmospheric moisture may also be relevant to hydroclimatic impacts, but these implications remain to be tested directly. Atmospheric moisture provides an important thermodynamic constraint on precipitation, while precipitation responses additionally depend on circulation, convection, cloud processes and storm dynamics (O'Gorman and Schneider 2009; Byrne and O'Gorman 2015; Pfahl et al. 2017; Ghausi et al. 2024). Observations also show widespread increases in heavy precipitation consistent with thermodynamic expectations (Fischer and Knutti 2016). The identification of a level-dependent transition in humidity realization therefore provides a testable basis for future work linking vertical moisture changes to precipitation extremes, drought and land-surface hydroclimate. The implications may extend beyond atmospheric humidity itself, given the documented links between warming, atmospheric moisture availability and drought risk over land (Dai 2013; Trenberth et al. 2014). The present results therefore provide a possible basis for future analyses linking vertically resolved humidity changes with precipitation extremes and other hydroclimatic responses, but they do not establish such relationships directly.

Several limitations constrain the interpretation. First, the residual is a diagnostic remainder rather than a complete moisture-budget decomposition and cannot uniquely quantify the contribution of individual physical processes. Second, the analysis is conducted on fixed pressure surfaces and therefore does not separately resolve changes associated with boundary-layer depth, tropopause height or other changes in vertical structure. Third, the C–C-based thermodynamic component is used as a local temperature-dependent reference rather than as a universal constraint on specific-humidity trends at every level or in every hydroclimatic regime. Finally, although the agreement among reanalysis products supports the broad diagnosed pattern, it cannot eliminate uncertainties inherent in long-term reanalysis humidity estimates.

Overall, terrestrial atmospheric moistening is better characterised by its height-dependent relationship to a temperature-related thermodynamic response than by a vertically uniform scaling with warming. The diagnosed residual is often substantial at lower levels and generally weakens toward the middle troposphere, while both components become small near 250 hPa. By resolving these relationships across hydroclimatic regimes, the study provides a framework for evaluating the vertical structure of long-term terrestrial specific-humidity change, while leaving the physical processes underlying the residual for future investigation.

Conclusions

Using ERA5 data from 1979 to 2025 across 37 pressure levels, together with consistency

assessments using MERRA-2 and ERA5-Land, this study reveals pronounced vertical variations in terrestrial atmospheric moistening and its thermodynamic and non-thermodynamic components. Specific-humidity increases are strongest in the lower troposphere, remain evident in the middle troposphere, and weaken substantially toward the upper troposphere.

The thermodynamic component is generally positive across the analysed pressure levels and hydroclimatic regimes, but the realized moistening is often smaller than the local Clausius–Clapeyron (C–C) scaling would suggest. Negative residuals substantially offset the thermodynamic component in the lower troposphere, become weaker toward the middle troposphere, and are small near 250 hPa, where the net specific-humidity trend approaches zero. This vertical pattern indicates that the realization of thermodynamic moistening potential varies with height.

Hydroclimatic contrasts further show that the realized response depends on the extent of residual offset, not simply on the magnitude of thermodynamic moistening potential. At 1000 hPa, for example, the hyperarid regime has a thermodynamic component of approximately +0.34 g kg^{-1} $decade^{-1}$ and a residual of −0.24 g kg^{-1} $decade^{-1}$, leaving a net increase of about +0.10–0.11 g kg^{-1} $decade^{-1}$. In the humid regime, a smaller thermodynamic component (+0.23 g kg^{-1} $decade^{-1}$) is nearly balanced by a residual of −0.21 g kg^{-1} $decade^{-1}$. The residual thus quantifies the difference between the observed trend and the thermodynamic component, although its individual physical contributions remain unresolved.

Overall, this study provides a vertically resolved framework for assessing how thermodynamic moistening potential is expressed in terrestrial atmospheric humidity changes. It offers a basis for evaluating climate-model simulations of specific-humidity trends, their deviations from local C–C scaling, and the vertical balance between thermodynamic and residual components. Further process-based moisture-budget analyses are needed to identify the physical processes underlying the residual.

Methods

Date

We using the fifth-generation European Centre for Medium-Range Weather Forecasts (ECMWF) Reanalysis (ERA5) as the primary atmospheric dataset. Monthly mean air temperature and specific humidity were obtained for 1979–2025 across 37 standard pressure levels from 1000 to 1 hPa at the native horizontal resolution of 0.25° × 0.25° (Hersbach et al. 2020) . The analysis period was selected to provide a consistent satellite-era framework while avoiding interpretation of reanalysis fields as direct observations. The consistency assessment of the principal results was assessed using MERRA-2 and ERA5-Land, with MERRA-2 used primarily to evaluate the vertical humidity response and ERA5-Land used to cross-check near-surface land specific-humidity trends (Gelaro et al. 2017; Muñoz-Sabater et al. 2021). ERA5 covers 1979–2025, whereas MERRA-2 covers 1980–2025; the consistency assessment uses the overlapping period.

Global terrestrial hydroclimatic regimes were defined using the UNEP-WCMC 2007 aridity dataset. Five regimes were identified according to the aridity index (AI = P/PET): Hyperarid (AI <

0.05), Arid ($0.05 \leq AI < 0.20$), Semiarid ($0.20 \leq AI < 0.50$), Drysubhumid ($0.50 \leq AI < 0.65$) and Humid ($AI \geq 0.65$) (UNEP-WCMC 2007). Antarctica south of 60°S was analysed separately as a reference region. Because fixed pressure surfaces can intersect the underlying topography, only grid cells located above the local surface were retained at each pressure level. Consequently, the spatial coverage decreases at lower pressure levels over high-elevation terrain and polar regions.

Monthly temperature and specific humidity were aggregated to annual means to emphasize long-term variability and reduce the influence of the seasonal cycle. The datasets were harmonized to a 1° × 1° grid, and longitudes were transformed to the −180° to 180° convention. Duplicate longitudes and invalid or missing values were removed during preprocessing. For regional analyses, grid-cell means were weighted by the cosine of latitude to account for differences in grid-cell area with latitude. ERA5, MERRA-2 and ERA5-Land were processed using consistent temporal and spatial conventions wherever applicable.

Vertical structure of specific humidity

The vertical structure of atmospheric moisture was quantified using the difference in specific humidity between adjacent pressure levels:

$$\Delta q = q_{p_l} - q_{p_u},$$

where (q_{p_l}) and (q_{p_u}) denote specific humidity at the lower-altitude (higher-pressure) and upper-altitude (lower-pressure) levels, respectively. Positive values indicate the typical tropospheric structure in which specific humidity decreases with height. Long-term trends in (Δq) were calculated to diagnose changes in the vertical moisture structure.

The vertical-gradient metric is used strictly as a diagnostic of humidity stratification and is not interpreted independently as a measure of convective intensity.

Trend estimation and significance testing

Long-term trends were estimated using the Theil–Sen median slope estimator, which is robust to non-normality and outliers. Statistical significance was assessed using the Hamed–Rao modified Mann–Kendall test to account for serial correlation in the time series. Trends with ($p < 0.05$) were considered statistically significant.

Unless otherwise stated, specific-humidity trends are reported in g kg^{-1} $decade^{-1}$. Spatial trend fields were calculated independently at each grid cell and pressure level, whereas regional values were obtained from cosine-latitude-weighted spatial means. Because the Theil–Sen estimator is not a linear operator, the trend of the residual is estimated independently and is not strictly constrained to equal the total trend minus the thermodynamic trend. Differences are small and do not affect the interpretation.

Clausius–Clapeyron-normalized humidity response

To compare humidity responses across pressure levels and hydroclimatic regimes, we calculated the specific-humidity trend normalized by the corresponding temperature trend:

$$R_q = \frac{dq/dt}{q_{clim} \cdot dT/dt} \times 100$$

where (dq/dt) is the specific-humidity trend and (q_{clim}) is the climatological specific humidity at the corresponding pressure level. The normalized response represents the fractional trend in specific humidity per unit temperature trend and is expressed in % K^{-1}.

The theoretical thermodynamic reference was based on local Clausius–Clapeyron scaling. The saturation vapour pressure sensitivity to temperature was calculated as

$$\frac{L_v}{R_v T^2}$$

where (L_v) is the latent heat of vaporization, (R_v) is the gas constant for water vapour and (T) is the climatological temperature. The resulting local C–C scaling was used as the pressure-level-specific thermodynamic reference. The conventional 7% K^{-1}scaling was retained as a fixed reference for comparison.

The C–C departure was defined as the difference between the observed normalized humidity response and the corresponding local C–C reference. Positive and negative values therefore indicate responses above and below the thermodynamic reference, respectively.

Thermodynamic component and non-thermodynamic residual

The temperature-driven thermodynamic component was calculated from the local sensitivity of saturation specific humidity to temperature:

$$\frac{\partial q_s}{\partial T} \approx q_s \frac{L_v}{R_v T^2}$$

where q_s is the saturation specific humidity at the local climatological temperature T (in Kelvin), L_v is the latent heat of vaporization (2.5×10^6 J kg^{-1}), and $R_v$is the specific gas constant for water vapour (461 J kg^{-1} K^{-1}). This expression assumes that the saturation vapour pressure is much smaller than the atmospheric pressure, a standard approximation for tropospheric conditions. The thermodynamic component time series is therefore defined as $Thermo_t = (q_s L_v / R_v T^2)\Delta T_t$, and its long-term trend is estimated using the same method as the total specific-humidity trend.

The observed specific-humidity trend is denoted as Total. The non-thermodynamic residual is then defined as $\mathrm{Total} - \mathrm{Thermo}$.

This thermodynamic component represents the change in saturation specific humidity induced by local temperature change under constant relative humidity. It is not the full temperature-driven

component of actual specific humidity, which would additionally involve the climatological relative humidity. The residual includes relative-humidity changes as well as other processes. Residual therefore represents the aggregate effect of processes not explicitly captured by the temperature-driven thermodynamic component. These processes may include changes in relative humidity, horizontal moisture transport and convergence, vertical motion, boundary-layer exchange and land–atmosphere interactions. Because the residual is defined diagnostically as the difference between the observed and thermodynamic components, it is not equivalent to an independent dynamical moisture-budget term and is not uniquely attributed to any individual circulation process.

Relative thermodynamic–residual diagnostics

Because the thermodynamic component and the non-thermodynamic residual can differ in both magnitude and direction of their effects on specific-humidity trends, three complementary diagnostics were used to characterize their relative balance across pressure levels and hydroclimatic regimes. These indices describe the relative magnitudes of the two components and are not interpreted as independent physical contributions to the moisture budget.

First, the thermodynamic–residual mean difference index (Thermodynamic–Residual Mean Difference Index (TMI)) was defined as

$$\mathrm{TMI} = \overline{\mathrm{Thermo}} - \overline{\mathrm{Residual}}$$

where the overbar denotes the spatial mean within a given hydroclimatic regime and pressure level. TMI retains the direction of the two components and therefore describes their mean magnitude contrast. Positive values indicate that the thermodynamic component exceeds the residual, whereas negative values indicate the opposite. TMI is not a fractional contribution to the total humidity trend.

Second, the component magnitude ratio (CR) was defined as

$$\log\left(\frac{|\mathrm{Thermo}| + \varepsilon}{|\mathrm{Residual}| + \varepsilon}\right)$$

where (ε) is a small positive constant introduced to avoid numerical instability when either component approaches zero. CR compares the absolute magnitudes of the two components. Thus, CR > 0 indicates a larger thermodynamic magnitude, whereas CR < 0 indicates a larger residual magnitude.

Third, the relative thermodynamic weight (W_{Thermo}) was defined as

$$\frac{|\mathrm{Thermo}|}{|\mathrm{Thermo}| + |\mathrm{Residual}|}$$

with values constrained between 0 and 1 when the denominator is non-zero. W_{Thermo} quantifies the fraction of the combined absolute magnitude represented by the thermodynamic component. Values approaching 1 indicate a larger relative thermodynamic magnitude, whereas values

approaching 0 indicate a larger residual magnitude. Importantly, W_{Thermo} is an absolute-magnitude weight rather than a contribution fraction to Total. This distinction is essential when Thermo and Residual have offset, as occurs frequently in the lower troposphere.

Together, TMI, CR and W_{Thermo} provide complementary information: TMI describes the mean difference, CR describes the logarithmic contrast in absolute magnitude, and W_{Thermo} expresses the thermodynamic component as a normalized absolute-magnitude weight. Their different mathematical definitions mean that the three indices are not expected to exhibit identical numerical patterns.

Data availability

The ERA5 reanalysis data used in this study are available from https://cds.climate.copernicus.eu/datasets/. The MERRA-2 reanalysis data are publicly available from the NASA Goddard Earth Sciences Data and Information Services Center (GES DISC; https://disc.gsfc.nasa.gov/). The MERRA-2 dataset is described in Gelaro et al. (2017, Journal of Climate, 30, 5419–5454, https://doi.org/10.1175/JCLI-D-16-0758.1), and the specific data products are cited with their respective DOIs in the text (Gelaro et al. 2017). The global dryland classification was obtained from UNEP-WCMC (2007), available at https://resources.unep-wcmc.org/products/789fcac8959943ab9ed7a225e5316f08. This dataset delineates global dryland areas based on an Aridity Index and classifies them into hyperarid, arid, semiarid, drysubhumid and humid zones following the UNCCD definition.

Code availability

The codes for creating the figures and analyses were written in Python Language Version 3.9.12. The source codes for the analysis of this study are available from the corresponding author upon reasonable request.

References

Allan, Richard P., and Hervé Douville. 2024. “An Even Drier Future for the Arid Lands.” *Proceedings of the National Academy of Sciences* 121 (2): e2320840121. https://doi.org/10.1073/pnas.2320840121.

Allan, Richard P., Kate M. Willett, Viju O. John, and Tim Trent. 2022. “Global Changes in Water Vapor 1979–2020.” *Journal of Geophysical Research: Atmospheres* 127 (12): e2022JD036728. https://doi.org/10.1029/2022JD036728.

Bony, Sandrine, Robert Colman, Vladimir M. Kattsov, et al. 2006. “How Well Do We Understand and Evaluate Climate Change Feedback Processes?” *Journal of Climate* 19 (15): 3445–82. https://doi.org/10.1175/JCLI3819.1.

Byrne, Michael P., and Paul A. O’Gorman. 2015. “The Response of Precipitation Minus Evapotranspiration to Climate Warming: Why the ‘Wet-Get-Wetter, Dry-Get-Drier’ Scaling Does Not Hold over Land*.” *Journal of Climate* 28 (20): 8078–92. https://doi.org/10.1175/JCLI-D-15-0369.1.

Byrne, Michael P., and Paul A. O'Gorman. 2018. "Trends in Continental Temperature and Humidity Directly Linked to Ocean Warming." *Proceedings of the National Academy of Sciences* 115 (19): 4863–68. https://doi.org/10.1073/pnas.1722312115.

Cao, Dingrui, Hai Lin, and Yi Huang. 2026. "Atmospheric Water Vapor Contribution to Interannual Variability of Northern Hemisphere Summer Heatwaves." *Npj Climate and Atmospheric Science* 9 (1): 88. https://doi.org/10.1038/s41612-026-01361-4.

Chung, Eui-Seok, Brian Soden, B. J. Sohn, and Lei Shi. 2014. "Upper-Tropospheric Moistening in Response to Anthropogenic Warming." *Proceedings of the National Academy of Sciences* 111 (32): 11636–41. https://doi.org/10.1073/pnas.1409659111.

Dai, Aiguo. 2013. "Increasing Drought under Global Warming in Observations and Models." *Nature Climate Change* 3 (1): 52–58. https://doi.org/10.1038/nclimate1633.

Dessler, A. E., and S. M. Davis. 2010. "Trends in Tropospheric Humidity from Reanalysis Systems." *Journal of Geophysical Research: Atmospheres* 115 (D19): 2010JD014192. https://doi.org/10.1029/2010JD014192.

Ding, Qinghua, Tiffany Shaw, Hailan Wang, Ian Baxter, and Jiang Zhu. 2026. "Regional Drying over the Western U.S. Driven by Enhanced Atmospheric Subsidence amid Global Moistening from 1980 to 2020." *Nature Communications* 17 (1): 5270. https://doi.org/10.1038/s41467-026-71818-w.

Douville, Hervé, B. Decharme, C. Delire, et al. 2020. "Drivers of the Enhanced Decline of Land Near-Surface Relative Humidity to Abrupt 4xCO2 in CNRM-CM6-1." *Climate Dynamics* 55 (5–6): 1613–29. https://doi.org/10.1007/s00382-020-05351-x.

Douville, Hervé, Saïd Qasmi, Aurélien Ribes, and Olivier Bock. 2022. "Global Warming at Near-Constant Tropospheric Relative Humidity Is Supported by Observations." *Communications Earth & Environment* 3 (1): 237. https://doi.org/10.1038/s43247-022-00561-z.

Fischer, E. M., and R. Knutti. 2016. "Observed Heavy Precipitation Increase Confirms Theory and Early Models." *Nature Climate Change* 6 (11): 986–91. https://doi.org/10.1038/nclimate3110.

Gelaro, Ronald, Will McCarty, Max J. Suárez, et al. 2017. "The Modern-Era Retrospective Analysis for Research and Applications, Version 2 (MERRA-2)." *Journal of Climate* 30 (14): 5419–54. https://doi.org/10.1175/JCLI-D-16-0758.1.

Ghausi, Sarosh Alam, Erwin Zehe, Subimal Ghosh, Yinglin Tian, and Axel Kleidon. 2024. "Thermodynamically Inconsistent Extreme Precipitation Sensitivities across Continents Driven by Cloud-Radiative Effects." *Nature Communications* 15 (1): 10669. https://doi.org/10.1038/s41467-024-55143-8.

Held, Isaac M., and Brian J. Soden. 2006. "Robust Responses of the Hydrological Cycle to Global Warming." *Journal of Climate* 19 (21): 5686–99. https://doi.org/10.1175/JCLI3990.1.

Hersbach, Hans, Bill Bell, Paul Berrisford, et al. 2020. “The ERA5 Global Reanalysis.” *Quarterly Journal of the Royal Meteorological Society* 146 (730): 1999–2049. https://doi.org/10.1002/qj.3803.

Jun, Tackseung, and David Rind. 2024. “Increasing Contribution of the Atmospheric Vertical Motion to Precipitation in a Warming Climate.” *Communications Earth & Environment* 5 (1): 541. https://doi.org/10.1038/s43247-024-01676-1.

Kim, Yeonuk, and Mark S. Johnson. 2025. “Deciphering the Role of Evapotranspiration in Declining Relative Humidity Trends over Land.” *Communications Earth & Environment* 6 (1): 105. https://doi.org/10.1038/s43247-025-02076-9.

Muñoz-Sabater, Joaquín, Emanuel Dutra, Anna Agustí-Panareda, et al. 2021. “ERA5-Land: A State-of-the-Art Global Reanalysis Dataset for Land Applications.” *Earth System Science Data* 13 (9): 4349–83. https://doi.org/10.5194/essd-13-4349-2021.

Novick, Kimberly A., Darren L. Ficklin, Charlotte Grossiord, et al. 2024. “The Impacts of Rising Vapour Pressure Deficit in Natural and Managed Ecosystems.” *Plant, Cell & Environment* 47 (9): 3561–89. https://doi.org/10.1111/pce.14846.

O’Gorman, P. A., and C. J. Muller. 2010. “How Closely Do Changes in Surface and Column Water Vapor Follow Clausius–Clapeyron Scaling in Climate Change Simulations?” *Environmental Research Letters* 5 (2): 025207. https://doi.org/10.1088/1748-9326/5/2/025207.

O’Gorman, Paul A., and Tapio Schneider. 2009. “The Physical Basis for Increases in Precipitation Extremes in Simulations of 21st-Century Climate Change.” *Proceedings of the National Academy of Sciences* 106 (35): 14773–77. https://doi.org/10.1073/pnas.0907610106.

Pfahl, S., P. A. O’Gorman, and E. M. Fischer. 2017. “Understanding the Regional Pattern of Projected Future Changes in Extreme Precipitation.” *Nature Climate Change* 7 (6): 423–27. https://doi.org/10.1038/nclimate3287.

Rodell, Matthew, and Bailing Li. 2023. “Changing Intensity of Hydroclimatic Extreme Events Revealed by GRACE and GRACE-FO.” *Nature Water* 1 (3): 241–48. https://doi.org/10.1038/s44221-023-00040-5.

Santer, B. D., C. Mears, F. J. Wentz, et al. 2007. “Identification of Human-Induced Changes in Atmospheric Moisture Content.” *Proceedings of the National Academy of Sciences* 104 (39): 15248–53. https://doi.org/10.1073/pnas.0702872104.

Schröder, Marc, Maarit Lockhoff, Lei Shi, et al. 2019. “The GEWEX Water Vapor Assessment: Overview and Introduction to Results and Recommendations.” *Remote Sensing* 11 (3): 251. https://doi.org/10.3390/rs11030251.

Seager, Richard, Naomi Naik, and Gabriel A. Vecchi. 2010. “Thermodynamic and Dynamic Mechanisms for Large-Scale Changes in the Hydrological Cycle in Response to Global

Warming*.” *Journal of Climate* 23 (17): 4651–68. https://doi.org/10.1175/2010JCLI3655.1.

Sherwood, S. C., R. Roca, T. M. Weckwerth, and N. G. Andronova. 2010. “Tropospheric Water Vapor, Convection, and Climate.” *Reviews of Geophysics* 48 (2): RG2001. https://doi.org/10.1029/2009RG000301.

Simpson, Isla R., Karen A. McKinnon, Daniel Kennedy, David M. Lawrence, Flavio Lehner, and Richard Seager. 2024. “Observed Humidity Trends in Dry Regions Contradict Climate Models.” *Proceedings of the National Academy of Sciences* 121 (1): e2302480120. https://doi.org/10.1073/pnas.2302480120.

Soden, Brian J., Darren L. Jackson, V. Ramaswamy, M. D. Schwarzkopf, and Xianglei Huang. 2005. “The Radiative Signature of Upper Tropospheric Moistening.” *Science* 310 (5749): 841–44. https://doi.org/10.1126/science.1115602.

Trenberth, Kevin E., Aiguo Dai, Gerard Van Der Schrier, et al. 2014. “Global Warming and Changes in Drought.” *Nature Climate Change* 4 (1): 17–22. https://doi.org/10.1038/nclimate2067.

UNEP-WCMC. 2007. “A Spatial Analysis Approach to the Global Delineation of Dryland Areas of Relevance to the CBD Programme of Work on Dry and Subhumid Lands.”

Vicente-Serrano, Sergio M., Raquel Nieto, Luis Gimeno, et al. 2018. “Recent Changes of Relative Humidity: Regional Connections with Land and Ocean Processes.” *Earth System Dynamics* 9 (2): 915–37. https://doi.org/10.5194/esd-9-915-2018.

Willett, Katharine M., Nathan P. Gillett, Philip D. Jones, and Peter W. Thorne. 2007. “Attribution of Observed Surface Humidity Changes to Human Influence.” *Nature* 449 (7163): 710–12. https://doi.org/10.1038/nature06207.

Wills, Robert C., Michael P. Byrne, and Tapio Schneider. 2016. “Thermodynamic and Dynamic Controls on Changes in the Zonally Anomalous Hydrological Cycle.” *Geophysical Research Letters* 43 (9): 4640–49. https://doi.org/10.1002/2016GL068418.

Zaitchik, Benjamin F., Matthew Rodell, Michela Biasutti, and Sonia I. Seneviratne. 2023. “Wetting and Drying Trends under Climate Change.” *Nature Water* 1 (6): 502–13. https://doi.org/10.1038/s44221-023-00073-w.

List of Figures

Figure 1: Vertical structure and evolution of terrestrial atmospheric specific humidity during the past 50 years. (a) Multi-year mean specific-humidity profiles across 37 standard pressure levels for five hydroclimatic regimes—Hyperarid, Arid, Semiarid, Drysubhumid and Humid—and the Antarctic regime. (b) Time–pressure evolution of specific-humidity anomalies over global land. (c–h) Corresponding time–pressure evolution for Hyperarid, Arid, Semiarid, Drysubhumid, Humid and Antarctic regimes, respectively. Anomalies are calculated relative to the corresponding climatological mean at each pressure level. Warm colours indicate positive anomalies (moistening), whereas cool colours indicate negative anomalies (drying)**.**

Figure 2: Long-term changes in the vertical gradient of terrestrial atmospheric specific humidity during the past 50 years. (a) Theil–Sen trends in the specific-humidity gradient (Δq) across the 1000–850, 850–500 and 500–250 hPa layers for the five hydroclimatic regimes and the Antarctic regime. (b–d) Global spatial distributions of the trends in Δq for the 500–250, 850–500 and 1000–850 hPa layers, respectively. Trends are expressed as g kg^{-1} $decade^{-1}$. Positive values indicate an increase in the vertical humidity contrast, whereas negative values indicate a weakening of the gradient. Only grid cells above the local surface are retained at each pressure level**.**

Figure 3: Vertical departures of terrestrial atmospheric moistening from Clausius–Clapeyron scaling and consistency assessment. (a) Vertical profiles of the observed temperature-trend-normalized specific-humidity trend (moistening rate) for the five hydroclimatic regimes and the Antarctic regime derived from ERA5 and MERRA-2. Coloured curves show regime-mean responses and shading indicates spatial variability. The grey dashed line denotes the conventional Clausius–Clapeyron scaling of 7% K^{-1}, whereas the black dash-dotted line represents the local temperature-dependent C–C scaling calculated for each pressure level. (b–d) Cross-product consistency assessment of specific-humidity trends from ERA5-Land and ERA5 at the 1000-hPa level. (b) Grid-cell comparison of Theil–Sen trends across the five hydroclimatic regimes; (c) spatial correlation between the two products; and (d) global distribution of trend differences between ERA5-Land and ERA5. Pressure levels above 250 hPa are shown for reference but are not included in the primary mechanistic interpretation**.**

Figure 4: Spatial and vertical partitioning of the C–C thermodynamic component and its residual over global land during the past 50 years. (a–d) Theil–Sen trends in specific humidity at 1000, 850, 500 and 250 hPa, respectively, expressed as g kg^{-1} $decade^{-1}$. (e) Thermodynamic components calculated from the local Clausius–Clapeyron sensitivity to temperature, representing the thermodynamic moistening potential under constant relative humidity. (f) Residuals after removing the C–C thermodynamic component, calculated as the observed specific-humidity trend minus the thermodynamic component. The residual represents the aggregate effect of processes not captured by the C–C saturation thermodynamic potential and is not interpreted as a direct contribution from any single physical process. (g) Spatial distributions of the thermodynamic component and residual across the selected pressure levels. (h) Vertical profiles of total, thermodynamic and residual trends for selected hydroclimatic regimes.

Figure 5: Hydroclimatic dependence of the vertical thermodynamic–residual balance in terrestrial atmospheric moisture during the past 50 years. (a–c) Specific-humidity trends at 1000, 850, 500 and 250 hPa for Antarctica and the five hydroclimatic regimes, shown as total trends (Total), C–C-based thermodynamic components (Thermo) and residuals after removing the C–C thermodynamic component (Residual). Total trends are expressed in g kg^{-1} $decade^{-1}$. Thermo represents the thermodynamic moistening potential under constant relative humidity, whereas Residual is defined as Total minus Thermo and represents the aggregate remainder not captured by the thermodynamic component. (d) Thermodynamic–residual mean difference index (TMI), defined as the difference between the regime-mean thermodynamic and residual components. (e) Logarithmic magnitude ratio, CR = log(|Thermo|/|Residual|), used to characterize the relative magnitude of the two components. Positive CR indicates a larger thermodynamic magnitude, whereas negative CR indicates a larger residual magnitude. The indices describe relative component magnitudes and should not be interpreted as contributions to the total trend.

Figure 6: Vertical variation in the relative thermodynamic weight and a conceptual synthesis

of terrestrial atmospheric moistening. (a) Vertical profiles of the thermodynamic weight, W_{Thermo} = |Thermo| / (|Thermo| + |Residual|), for the five hydroclimatic regimes and Antarctica. W_{Thermo} ranges from 0 to 1 and quantifies the relative absolute magnitude of the thermodynamic component compared with the C–C residual. Crosses indicate levels where Thermo and Residual have offset. High W_{Thermo} values therefore indicate greater thermodynamic magnitude but do not necessarily imply a positive thermodynamic compon ent to the net humidity trend. (b) Conceptual synthesis of the three-stage vertical response: a lower-tropospheric compensation zone characterized by strong thermodynamic–residual compensation; a middle-tropospheric thermodynamic-expression zone where the residual weakens and the thermodynamic signal becomes more directly expressed; and an upper-tropospheric weak-response zone where both components decline toward small absolute magnitudes**.**

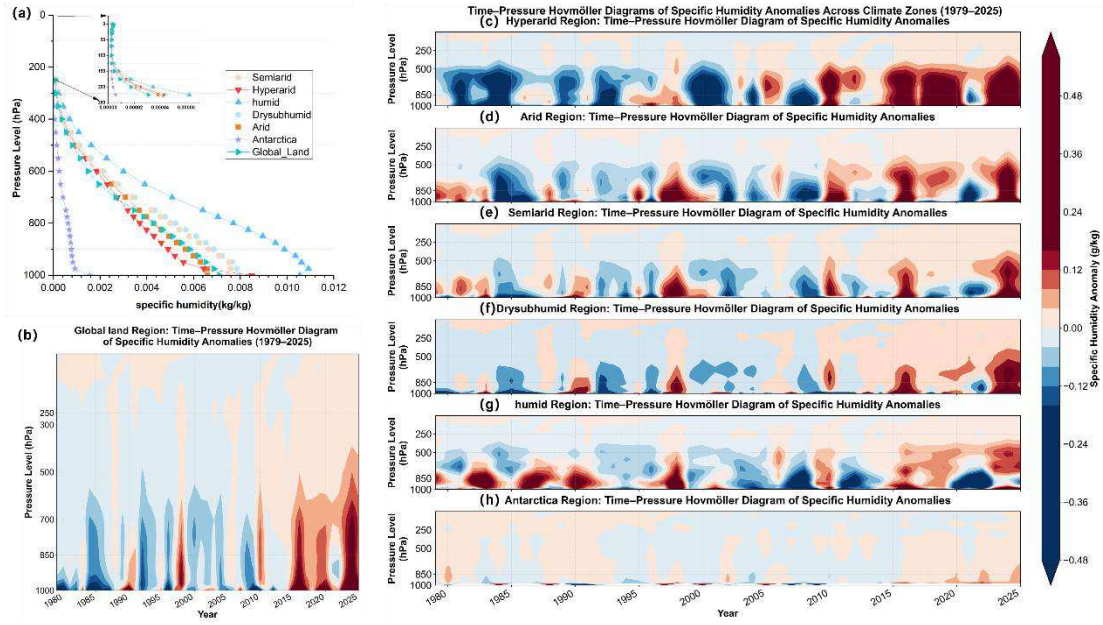


Figure 1

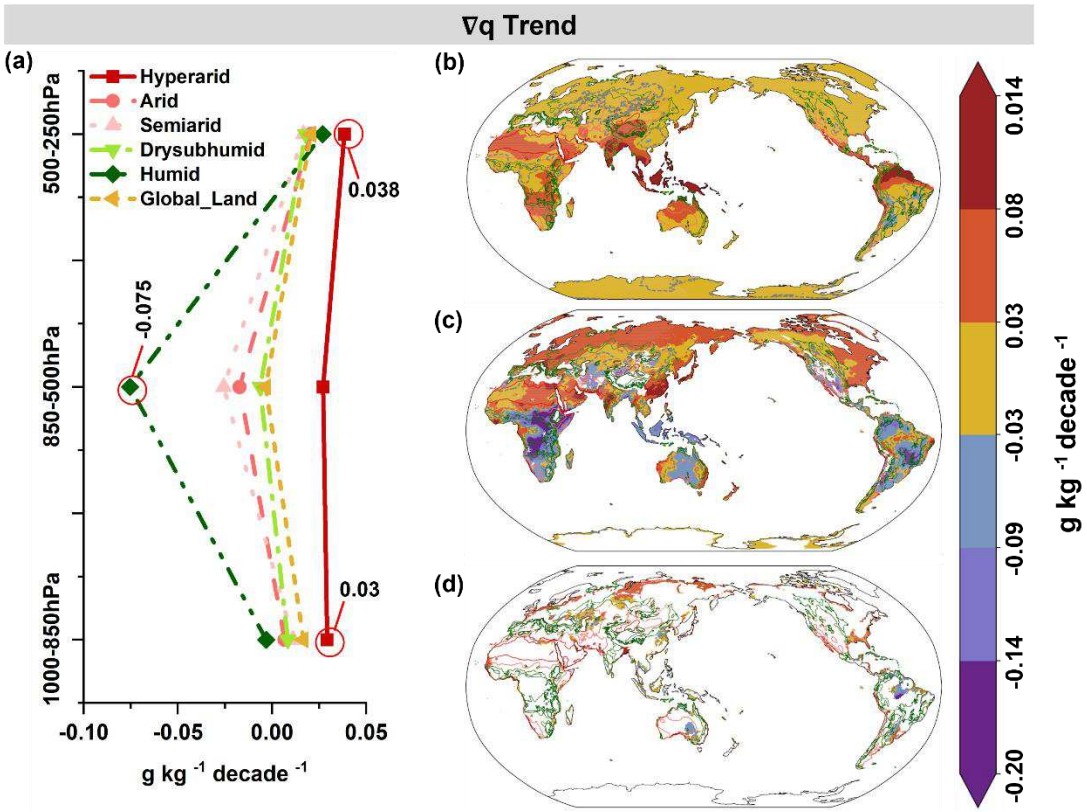


Figure 2

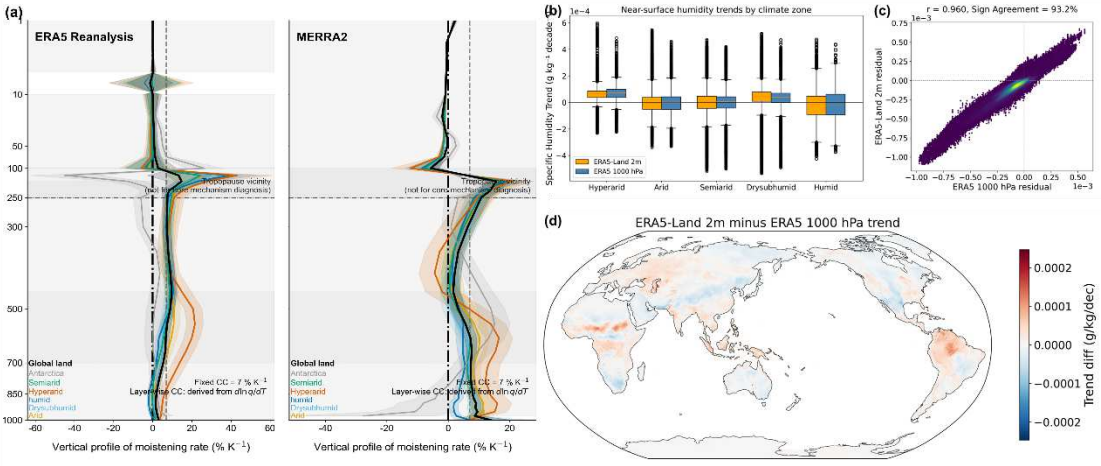


Figure 3

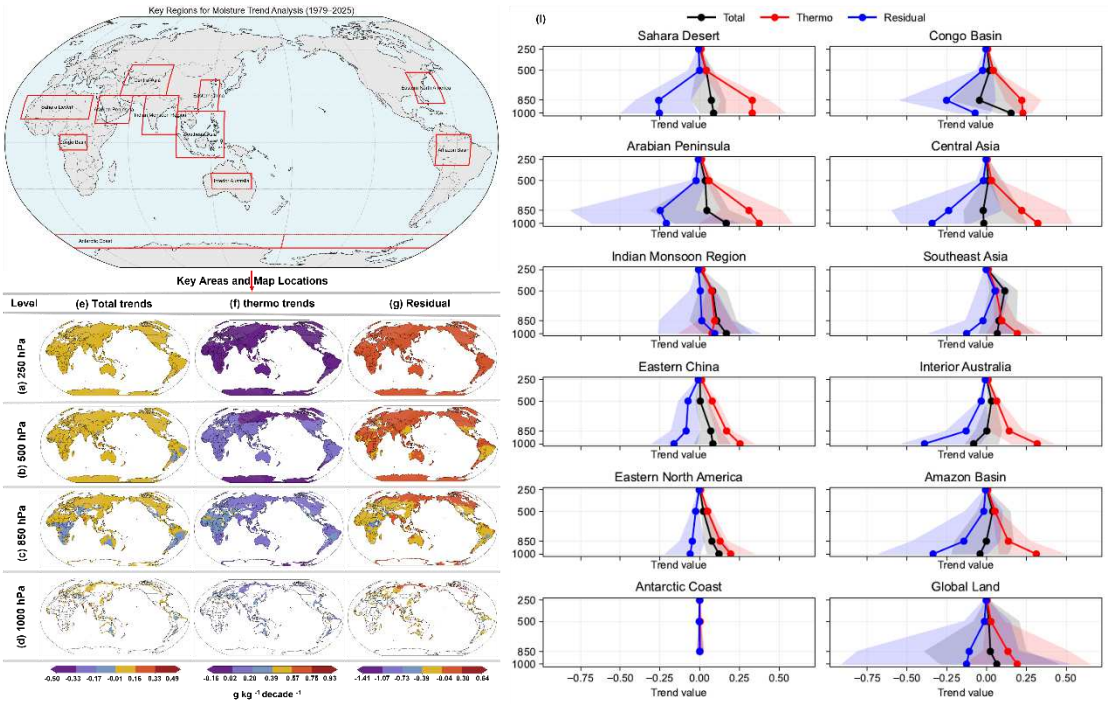


Figure 4

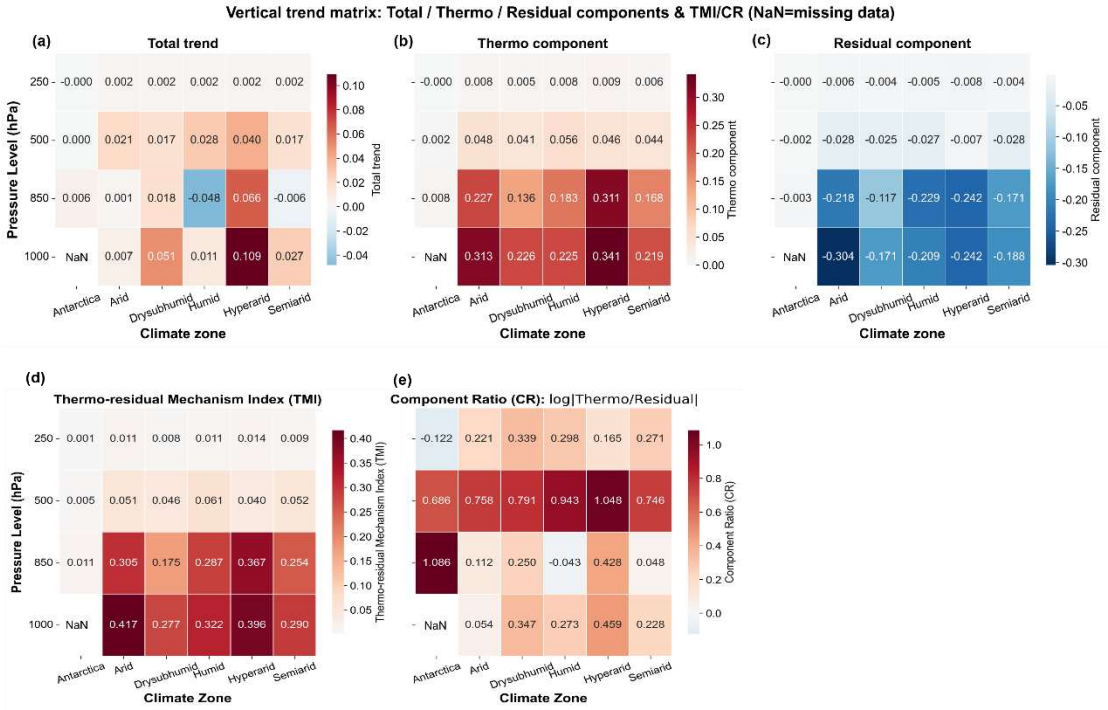


Figure 5

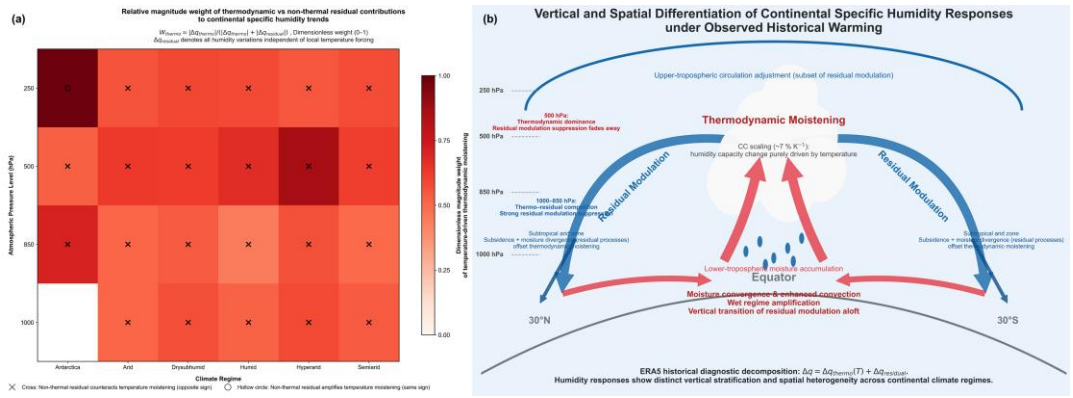


Figure 6

Funding

This work was supported by the National Natural Science Foundation of China (Grant No. 42271007). the National Key R&D Program of China (Grant No. 2022YFF1302401).

Author contributions

S.X. and H.H. conceived the study and developed the methodology. S.X. conducted the investigation and performed the formal analysis. S.X. and J.Z. prepared the figures and visualizations. S.X., H.H., and J.Z. supervised the research. S.X. wrote the original draft of the manuscript. S.X., H.H., and J.Z. reviewed and edited the manuscript. All authors have read and approved the manuscript.

Competing financial interests

The author declares no competing financial interests.

Supplementary Files

This is a list of supplementary files associated with this preprint. Click to download.

- GraphicalAbstract.png